2026 IEEE International Conference on Robotics and Automation (ICRA 2026)
June 1-5, 2026. Vienna, Austria

Adaptive Physical Human–Robot Interaction via a Passivity-Aware Model Predictive Variable Admittance Control

Dalia M. Mahfouz *Member, IEEE,*[1,2], Paolo Di Lillo *Member, IEEE,*[3],
Omar M. Shehata *Member, IEEE,* [1,2], Elsayed I. Morgan[1,2] and Filippo Arrichiello *Senior Member, IEEE,*[3]

***Abstract*— Physical Human–Robot Interaction (pHRI) requires control frameworks that balance accuracy, compliance, and safety under variable human behaviors. This paper proposes a novel Model Predictive Variable Admittance (MPVA) framework that integrates trajectory tracking, interaction force directionality, and passivity constraints into an online real-time optimization scheme. The proposed architecture is implemented on a 7-DoF Kinova Jaco-2 robot and validated experimentally through mixed assistive and resistive modes with multiple subjects performing pHRI tasks. Results supported by both objective metrics and subjective evaluation through a NASA TLX survey show that the MPVA achieves competitive tracking accuracy, reducing physical effort with minimal passivity violations compared to other algorithmic baselines such as fixed-gain admittance and fuzzy-based adaptive admittance. This demonstrates safe and effective human-robot physical interaction across diverse modes.**

***Index Terms*— Variable admittance control, Model predictive, Fuzzy-based, Intent-aware, Safety, Physical human-robot interaction.**

1. Introduction

Physical Human-Robot Interaction (pHRI) has gained increasing attention across a wide range of robotic applications, including industrial manufacturing, rehabilitation, agriculture, and others [1], [2]. As robotic systems are increasingly deployed in unstructured environments shared with humans, it becomes essential for robots to physically engage and interact with human partners. This interaction enhances task efficiency, adaptability, and user acceptance, while also adding the need to properly address the inherent variability of human behavior and the critical importance of safety [1]. Thus, one of the main challenges is to provide a control framework that can assist human motion, ensuring comfortable, responsive, and intuitive interaction while maintaining accurate path tracking and avoiding resistive behavior or instability [3].

This work was supported by Project COM^3 CUP H53D23000610006 funded by EU in NextGenerationEU plan through the Italian "Bando Prin 2022 - D.D. 104 del 02-02-2022" by MUR, and by the Italian Ministry of Research, under the complementary actions to the NRRP "Fit4MedRob - Fit for Medical Robotics" Grant PNC0000007. The experiments were taken in accordance with the Declaration of Helsinki, the protocol has been approved by the Research Ethics Committee of the University of Cassino and Southern Lazio and the subjects gave informed consent.

[1]Mechatronics Dept., Faculty of Engineering and Materials Science, German University in Cairo, Egypt, {dalia.mahfoz, omar.mohamad, elsayed.morgan}@guc.edu.eg

[2]Multi-Robot Systems (MRS) Research Group, Cairo, Egypt

[3]Department of Electrical and Information Engineering (DIEI), University of Cassino and Southern Lazio, Italy, {pa.dilillo, f.arrichiello}@unicas.it

Admittance control is a widely adopted strategy for pHRI applications that establishes a dynamic relationship between external human–robot interaction forces and robot motion [4], supporting natural and smooth collaboration [5]. However, inappropriate selection of admittance parameters may lead to instability, unsafe behavior, or degraded performance, especially under variable human motion and intent. To address these limitations, recent research has focused on *variable admittance control*, where inertia, damping, and stiffness are adjusted online using real-time interaction metrics. Early heuristic self-switching methods alternated between interaction or control modes (e.g., position/force control) to accommodate varying assistance or resistance [6], but these approaches can introduce discontinuities and lack formal safety guarantees. Continuous gain-scheduling strategies [7], [8] instead adapt parameters using linear or weighted functions of interaction forces and tracking deviations; however, they neglect force directionality, which is essential for interpreting human intent and ensuring motion alignment. Fuzzy-based adaptation has been widely used in pHRI to encode expert knowledge without detailed HRI models [9]. In [10], fuzzy adaptation effectively captured force magnitude and directionality for intent-aware adjustment. Nevertheless, fuzzy logic lacks predictive capability and cannot guarantee stability or safety in dynamic interactions. Model Predictive Control (MPC) has therefore emerged as a promising alternative, enabling multi-objective optimization under system constraints. MPC-based approaches have been used to adapt admittance/impedance parameters to minimize tracking error, improve compliance, and maintain stability under interaction forces [11]–[13]. However, most existing work emphasizes tracking accuracy and compliance without explicitly considering interaction force directionality, and, to the best of our knowledge, none implicitly integrate human safety conditions within the control objectives and constraints.

To address these challenges, this paper proposes a Model Predictive Variable Admittance (MPVA) strategy based on an MPC adaptation scheme for computing admittance parameters. The MPVA formulation minimizes tracking error, augments the cost with interaction force information for intent-aware adaptation, and incorporates safety constraints through passivity analysis [14]. The proposed architecture is novel for adaptive admittance control in pHRI, enabling smooth intent-aware adaptation while regulating energy exchange to prevent unsafe interactions.

By examining MPVA alongside the fuzzy-based formulation in [10], this work provides insight into the trade-offs between heuristic and optimization-based strategies for accurate, compliant, and safe physical interaction. Specifically, the study aims to: i) develop a real-time MPVA framework integrating trajectory tracking, force directionality, and passivity constraints for safe intent-aware pHRI; ii) systematically compare fuzzy-based adaptation with the proposed MPVA within a unified framework; and iii) experimentally validate performance across multiple subjects on planar and rehabilitation-inspired 3D trajectories under assistive/resistive behaviors, revealing trade-offs in accuracy, complexity, compliance, and safety.

The rest of the paper is organized as follows: Section 2 outlines the control framework. The admittance parameter adaptation strategy is detailed in section 3. Section 4 presents and discusses the results. Finally, section 5 concludes the work and recommends future endeavors.

2. Proposed Control Framework

The proposed framework comprises three modules: 1) a hierarchical control scheme that applies admittance control at the task level, modeling HRI as a virtual mass–spring–damper driven by human forces and generating a desired end-effector trajectory tracked by a joint-level controller; 2) an MPC-based adaptation module that updates admittance parameters online; and 3) a human interpretation module that analyzes tracking deviation, interaction forces, and their directionality to support adaptation. Together, these modules balance tracking performance, compliance during assistance, and stability during resistance, ensuring safe pHRI. The overall structure is shown in Fig. 1. The hierarchical control scheme includes: i) a variable admittance controller that modifies the *reference* trajectory using force/torque measurements to produce a *desired* trajectory; ii) an inverse kinematics module that computes required joint velocities; and iii) a joint-level controller that generates commanded velocities using encoder feedback.

A. Inverse Kinematics and Joint-Level Control

Consider a serial robotic manipulator with n degrees of freedom. Its configuration is described by the joint position vector $\boldsymbol{q} = [q_1, q_2, \cdots, q_n]^T \in \mathbb{R}^n$. The end-effector state is encoded in the vector $\boldsymbol{x} = \begin{bmatrix}\boldsymbol{p}^T & \boldsymbol{o}^T\end{bmatrix}^T \in \mathbb{R}^7$, where $\boldsymbol{p} \in \mathbb{R}^3$ contains the position coordinates and $\boldsymbol{o} \in \mathbb{R}^4$ represents orientation in quaternion form, both expressed in the base frame. The end-effector velocity is represented by $\boldsymbol{v} = \begin{bmatrix}\dot{\boldsymbol{p}}^T & \boldsymbol{\omega}^T\end{bmatrix}^T \in \mathbb{R}^6$, combining the translational velocity $\dot{\boldsymbol{p}} \in \mathbb{R}^3$ and angular velocity $\boldsymbol{\omega} \in \mathbb{R}^3$. These velocities are related to the joint velocities $\dot{\boldsymbol{q}} \in \mathbb{R}^n$ through the Jacobian matrix $\boldsymbol{J} \in \mathbb{R}^{6\times n}$ as $\boldsymbol{v} = \boldsymbol{J}\dot{\boldsymbol{q}}$. In the case of a redundant manipulator (i.e., $n > 6$), and assuming a desired trajectory in the operational space defined by:

$$\boldsymbol{x}_d = \begin{bmatrix}\boldsymbol{p}_d \\ \boldsymbol{o}_d\end{bmatrix} \in \mathbb{R}^7 \quad \boldsymbol{v}_d = \begin{bmatrix}\dot{\boldsymbol{p}}_d \\ \boldsymbol{\omega}_d\end{bmatrix} \in \mathbb{R}^6 \quad \boldsymbol{a}_d = \begin{bmatrix}\ddot{\boldsymbol{p}}_d \\ \boldsymbol{\alpha}_d\end{bmatrix} \in \mathbb{R}^6 \tag{1}$$

the joint velocities needed to follow the path are obtained using the Closed-Loop Inverse Kinematics (CLIK) [15] as $\dot{\boldsymbol{q}}_d = \boldsymbol{J}^\dagger (\boldsymbol{v}_d + \boldsymbol{K}_{\text{ik}}\tilde{\boldsymbol{x}})$, where $\boldsymbol{J}^\dagger$ denotes the Moore-Penrose pseudoinverse of $\boldsymbol{J}$, $\boldsymbol{K}_{\text{ik}} \in \mathbb{R}^{6\times 6}$ is a gain matrix, and $\tilde{\boldsymbol{x}}$ denotes the tracking error in operational space as $\tilde{\boldsymbol{x}} = \begin{bmatrix}\tilde{\boldsymbol{p}}^T, \tilde{\boldsymbol{o}}^T\end{bmatrix}^T = \begin{bmatrix}(\boldsymbol{p}_d - \boldsymbol{p}(\boldsymbol{q}_d))^T, (\boldsymbol{o}_d^{-1} \star \boldsymbol{o}(\boldsymbol{q}_d))^T\end{bmatrix}^T \in \mathbb{R}^6$ where $\tilde{\boldsymbol{p}}$ and $\tilde{\boldsymbol{o}}$ represent position and orientation errors, respectively, and $\star$ indicates quaternion multiplication. The vector $\boldsymbol{q}_d$ is the desired joint configuration obtained by integrating $\dot{\boldsymbol{q}}_d$, while $\boldsymbol{p}(\boldsymbol{q}_d)$ and $\boldsymbol{o}(\boldsymbol{q}_d)$ are the direct kinematic mappings of the end-effector pose.

Finally, the desired joint velocities $\dot{\boldsymbol{q}}_d$ are tracked by the joint controller, which applies a proportional control strategy with feedforward as $\dot{\boldsymbol{q}}_r = \dot{\boldsymbol{q}}_d + \boldsymbol{K}_{\text{jc}}\tilde{\boldsymbol{q}}$, where $\boldsymbol{K}_{\text{jc}} \in \mathbb{R}^{n\times n}$ is a positive-definite gain matrix and $\tilde{\boldsymbol{q}} = \boldsymbol{q}_d - \boldsymbol{q}$ is the joints position error based on encoder measurements.

B. Variable Admittance Controller

The objective of the admittance controller is to impose a virtual mechanical behavior on the end-effector of the manipulator, characterized by specified mass, stiffness and friction. Assuming the availability of a reference trajectory for the end-effector and measurements from a wrist-mounted force/torque sensor, the desired dynamics of the system can be formalized as:

$$\boldsymbol{K}_m\, \tilde{\boldsymbol{a}}_{r,d} + \boldsymbol{K}_d\, \tilde{\boldsymbol{v}}_{r,d} + \boldsymbol{K}_k\, \tilde{\boldsymbol{x}}_{r,d} = \boldsymbol{h}; \tag{2}$$

where $\boldsymbol{h} = \begin{bmatrix}\boldsymbol{f}^T & \boldsymbol{\mu}^T\end{bmatrix}^T \in \mathbb{R}^6$ is the external wrench vector (forces and torques), $\boldsymbol{K}_m = \text{diag}(\boldsymbol{K}_m^p, \boldsymbol{K}_m^o)$, $\boldsymbol{K}_d = \text{diag}(\boldsymbol{K}_d^p, \boldsymbol{K}_d^o)$ and $\boldsymbol{K}_k = \text{diag}(\boldsymbol{K}_k^p, \boldsymbol{K}_k^o)$ are the virtual inertia, damping, and stiffness matrices, with translational and rotational sub-blocks denoted accordingly. The associated errors between the *reference* (r) and *desired* (d) are:

$$\tilde{\boldsymbol{x}}_{r,d} = \begin{bmatrix}\boldsymbol{p}_r - \boldsymbol{p}_d \\ \boldsymbol{o}_r^{-1} \star \boldsymbol{o}_d\end{bmatrix}, \tilde{\boldsymbol{v}}_{r,d} = \boldsymbol{v}_r - \boldsymbol{v}_d, \tilde{\boldsymbol{a}}_{r,d} = \boldsymbol{a}_r - \boldsymbol{a}_d \tag{3}$$

By substituting Eqs. (3) into Eq. (2) and solving for $\boldsymbol{a}_d$, one obtains $\boldsymbol{a}_d = \boldsymbol{K}_m^{-1}\left[\boldsymbol{K}_m\boldsymbol{a}_r + \boldsymbol{K}_d\tilde{\boldsymbol{v}}_{r,d} + \boldsymbol{K}_k\tilde{\boldsymbol{x}}_{r,d} - \boldsymbol{h}\right]$, where the desired velocity $\boldsymbol{v}_d$ and pose $\boldsymbol{x}_d$ are obtained by integrating $\boldsymbol{a}_d$. Adapting $\boldsymbol{K}_m$, $\boldsymbol{K}_d$, and $\boldsymbol{K}_k$ in real-time allows the realization of a variable admittance behavior.

3. Admittance Parameters Adaptation

In physical human–robot interaction (pHRI), the choice of admittance parameters is critical for balancing responsiveness, stability, and user comfort. Fixed gains often fail to accommodate variations in human input, leading to either sluggish tracking or unsafe oscillations. To overcome these limitations, an adaptive scheme is proposed to adjust the admittance gains online. The adaptive admittance scheme employed is based on an optimization-based strategy, which is implemented using Model Predictive Control (MPC) formulation. This strategy relys on human-interpreted data extracted during physical interaction, including the tracking error, the magnitude of the interaction force, and its direction relative to the desired motion. In this section, the interpreted data are introduced. In addition, we detail the MPC-based adaptation method considered in this work.

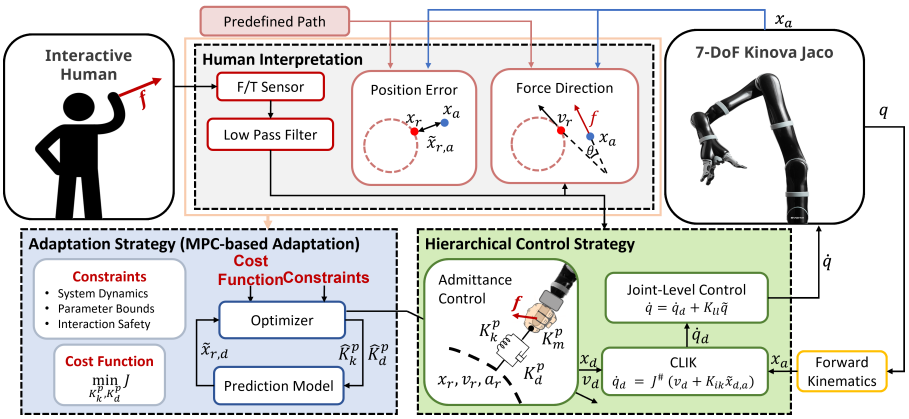

Fig. 1: Variable Admittance Control Framework

A. Human-interpreted data

The proposed adaptation framework relies on real-time human-interpreted data that characterizes the interaction between the human and the robot. The data is driven by three primary factors: the tracking error $\tilde{\boldsymbol{x}}_{r,d}$, the magnitude of the applied external wrench $|\boldsymbol{h}|$, and its direction with respect to the track to estimate both assistive and resistive human behavior, as shown in the human interpretation module in Fig. 1. In this formulation, the applied torques are neglected $\boldsymbol{\mu} = \mathbf{0}$ under the assumption of a rigid human grasp with no wrist articulation, allowing the focus to remain solely on the translational interaction forces $\boldsymbol{f} = [f_x, f_y, f_z]^T \in \mathbb{R}^3$. The direction of the applied force $\cos(\theta)$ is computed relative to the nearest reference velocity $\boldsymbol{v}_r$ to the robot's pose:

$$\cos(\theta) = \frac{\boldsymbol{f} \cdot \boldsymbol{v}_r}{|\boldsymbol{f}||\boldsymbol{v}_r|} = \begin{cases} > 0, & \text{assistive} \\ \leq 0, & \text{resistive} \end{cases} \tag{4}$$

A positive value of $\cos(\theta)$ indicates assistive behavior as the applied forces are aligned with the desired motion, while a negative value denotes resistive behavior as the applied forces are opposing or orthonormal to the motion direction. These interpreted quantities are used as inputs to the adaptation strategy, where the MPC-based adaptation incorporates them into the optimization objectives and constraints.

B. MPC-based adaptation strategy

A model-based adaptation technique is developed to adjust the admittance parameters online. This technique is based on the Model Predictive Control (MPC) principle, which considers the system dynamics, handles multiple constraints, and optimizes the control input over a prediction horizon N_p. The MPC is employed to compute the optimal position-related admittance stiffness $\boldsymbol{K}_k^p = \text{diag}(k_{k_x}, k_{k_y}, k_{k_z}) \in \mathbb{R}^{3\times3}$ and damping $\boldsymbol{K}_d^p = \text{diag}(k_{d_x}, k_{d_y}, k_{d_z}) \in \mathbb{R}^{3\times3}$ control parameters that best accommodate the human behavior while ensuring compliant and stable interaction. Based on the rigid human grasp assumption, the orientation-related admittance parameters are kept constant throughout the interaction. This assumption simplifies the optimization problem by reducing the dimensionality of the decision space while remaining sufficient for various HRI tasks.

Nevertheless, the framework is extendable to handle the possible applied torques. The proposed Model Predictive Variable Admittance (MPVA) control takes into account the tracking error focusing on motion accuracy, the human-applied forces allowing the controller to adapt in an intent-aware manner, and the passivity constraints, ensuring that the robot does not inject energy into the interaction, which is important to guarantee safety during physical contact. The admittance dynamic model used in the prediction stage of the MPC formulations is represented through Eq. (2). The virtual damping and stiffness of the interaction in Cartesian space are treated as decision variables in the MPC optimization, while the virtual inertia is fixed as a positive definite diagonal matrix $\boldsymbol{K}_m^p = \text{diag}(k_{m_x}, k_{m_y}, k_{m_z}) \in \mathbb{R}^{3\times3}$. To embed the admittance dynamics into the predictive model, the system is expressed in a continuous-time state–space form with position and velocity deviations $\boldsymbol{x}(t) = [\tilde{\boldsymbol{x}}_{r,d}^{p\top}, \tilde{\boldsymbol{v}}_{r,d}^{p\top}]^T$ under the influence of the external interaction forces $\boldsymbol{f}$ as:

$$\boldsymbol{A}_c = \begin{bmatrix} \mathbf{0} & \mathbf{1} \\ -\boldsymbol{K}_k^p \boldsymbol{K}_m^{p^{-1}} & -\boldsymbol{K}_d^p \boldsymbol{K}_m^{p^{-1}} \end{bmatrix}, \quad \boldsymbol{B}_c = \begin{bmatrix} \mathbf{0} \\ \boldsymbol{K}_m^{p^{-1}} \end{bmatrix} \tag{5}$$

where $\boldsymbol{A}_c$ and $\boldsymbol{B}_c$ are the continuous state transition and input matrices, respectively. This continuous-time model is discretized using forward Euler method to obtain $\boldsymbol{A}_d$ and $\boldsymbol{B}_d$, which are used to predict the system evolution over the horizon. Both $\boldsymbol{A}_d$ and $\boldsymbol{B}_d$ vary dynamically with the optimized stiffness and damping, directly coupling the adaptation method to the predictive model.

The cost function J_c penalizes tracking error and interaction forces across the prediction horizon:

$$\min_{K_k^p, K_d^p} J_c = \sum_{k=0}^{N_p-1} \Big[\|\tilde{\boldsymbol{x}}_{r,d}^p(k)\|_{\boldsymbol{Q}}^2 + \|\boldsymbol{K}_k^p(k) - \boldsymbol{K}_{k_t}^p(k)\|_{\boldsymbol{R}_k}^2 + \|\boldsymbol{K}_d^p(k) - \boldsymbol{K}_{d_t}^p(k)\|_{\boldsymbol{R}_d}^2 + \beta \|s(k)\|^2 \Big] + \|\tilde{\boldsymbol{x}}_{r,d}^p(N_p)\|_{\boldsymbol{Q}_n}^2 \tag{6}$$

$$\text{s.t.} \quad \boldsymbol{x}(k+1) = \boldsymbol{A}_d(k)\boldsymbol{x}(k) + \boldsymbol{B}_d \boldsymbol{f}(k) \tag{7}$$

$$k_{\min} \leq \boldsymbol{K}_k^p(k) \leq k_{\max} \tag{8}$$

$$\boldsymbol{K}_d^p(k) \geq \boldsymbol{K}_{d_t}^p(k) \tag{9}$$

$$\tilde{\boldsymbol{x}}_{r,d}^{p\top}(k) \Delta \boldsymbol{K}_k^p(k) \tilde{\boldsymbol{x}}_{r,d}^p(k) - \tilde{\boldsymbol{v}}_{r,d}^{p\top}(k) \boldsymbol{K}_d^p(k) \tilde{\boldsymbol{v}}_{r,d}^p(k) \leq s(k) \tag{10}$$

where the sampling instant is denoted as k, $\boldsymbol{Q}$ and $\boldsymbol{Q}_n \in \mathbb{R}^{3\times3}$ are positive definite weighting matrices used to penalize the tracking error over the prediction horizon N_p and at the final step, respectively. The positive definite weighting matrices $\boldsymbol{R}_k$ and $\boldsymbol{R}_d \in \mathbb{R}^{3\times3}$ are used to penalize the deviations of the current stiffness and damping parameters from their designed target profiles $\boldsymbol{K}^p_{k_t}$ and $\boldsymbol{K}^p_{d_t}$, respectively. The positive scalar weight β is used to serve as a weighting coefficient for the slack variable $s(k)$, which is presented to relax the hard constraints and ensure the feasibility of the optimization process.

To clarify and emphasize the contribution of the terms presented, each term is discussed separately.

1) Tracking Term: It represents the first and the last terms in the cost function in Eq. (6), which minimize $\|\tilde{\boldsymbol{x}}^p_{r,d}(k)\|^2_{\boldsymbol{Q}}$ and $\|\tilde{\boldsymbol{x}}^p_{r,d}(N_p)\|^2_{\boldsymbol{Q}_n}$ to ensure accurate trajectory and steady-state tracking, respectively.

2) Stiffness Adaptation Term: The second term in the cost function expressed as $\|\boldsymbol{K}^p_k(k) - \boldsymbol{K}^p_{k_t}(k)\|^2_{\boldsymbol{R}_{K_k}}$, is used to penalize the deviation of the current stiffness parameter from a target stiffness profile in the Cartesian space $\boldsymbol{K}^p_{k_t} = \text{diag}(k_{k_{x_t}}, k_{k_{y_t}}, k_{k_{z_t}}) \in \mathbb{R}^{3\times3}$, which is continuously computed at each sample k. The computation of the target stiffness profile is introduced to guide real-time parameters adaptation based on human assistive and resistive physical interactions. The target stiffness $\boldsymbol{K}^p_{k_{i_t}}$ of the i^{th} Cartesian axis is defined as a function of the applied force magnitude and its alignment to the reference path:

$$\boldsymbol{K}_{k^p_{i_t}}(k) = \begin{cases} k_{\min} + 0.5\ \delta_1\ (1-\phi(k))\boldsymbol{f}_n, \text{ assist} \\ k_{\max} + 0.5\ \delta_2\ (1-\phi(k))\boldsymbol{f}_n, \text{ resist} \end{cases} \tag{11}$$

where $\delta_1 = k_{\max} - k_{\min}$, $\delta_2 = k_{\min} - k_{\max}$ with $k_{\max}$ and $k_{\min}$ being the maximum and minimum bounds of the desired virtual stiffness, $\phi(k) = |\cos(\theta(k))|$ which is calculated in Eq. (4) representing the force direction and $\boldsymbol{f}_n$ is the normalized applied force magnitude calculated as $\boldsymbol{f}_n = (\boldsymbol{f} - f_{\min})/(f_{\max} - f_{\min})$, where $f_{\max}$ and $f_{\min}$ are the bounds of applied human force magnitudes.

3) Damping Adaptation Term: The third term in the cost function, expressed as $\|\boldsymbol{K}^p_d(k) - \boldsymbol{K}^p_{d_t}(k)\|^2_{\boldsymbol{R}_{K_d}}$, is used to regularize the damping parameter adaptation to converge to the assigned target damping profile $\boldsymbol{K}^p_{d_t}(k) = \text{diag}(k_{dx_t}, k_{d_{y_t}}, k_{d_{z_t}}) \in \mathbb{R}^{3\times3}$. The target damping $\boldsymbol{K}^p_{d_{t_i}}(k)$ is set based on the corresponding i^{th} component of the computed optimal stiffness $\boldsymbol{K}^p_{k_i}(k)$ and of the fixed inertia term $\boldsymbol{K}^p_{m_i}$ in each time sample k to ensure a critically damped behavior, such that $(K^p_{d_{i_t}}(k) = 2\sqrt{K^p_{m_i} K^p_{k_i}(k)}); i = x, y, z$. The damping term incorporated within the cost function leads to the response convergence with minimal overshoot, while maintaining safety and comfort in the pHRI.

4) Slack Variable Penalty: The fourth term in the cost function, denoted as $\beta\|s(k)\|^2$, is used to soften the system's safety constraints with a non-negative slack variable $s(k) > 0$. The penalty weight β determines the trade-off between strict safety enforcement and tracking performance.

The optimization problem is characterized by several constraints, which are the system dynamics constraint in Eq. (7), stiffness bounds constraint in Eq. (8) to ensure safe and feasible range, and minimum damping constraint in Eq. (9) to ensure a critically damped to overdamped system. In addition, the safety constraint in Eq. (10) enforces the passivity of the system, which is used to guarantee the system's stability and safety in the presence of human physical interaction. Indeed, this property prevents unstable or aggressive robot behaviors that can harm the human user. Passivity is guaranteed if the energy dissipated by the system's damping component $\tilde{\boldsymbol{v}}^{p\top}_{r,d}(k)\boldsymbol{K}^p_d(k)\tilde{\boldsymbol{v}}^p_{r,d}(k)$ exceeds or matches the energy stored by the time-varying stiffness rate $\tilde{\boldsymbol{x}}^{p\top}_{r,d}(k)\Delta\boldsymbol{K}^p_k(k)\tilde{\boldsymbol{x}}^p_{r,d}(k)$. The rate of change of the time-varying stiffness in each sample k is defined as $\Delta\boldsymbol{K}^p_k(k) \in \mathbb{R}^{3\times3}$. This inequality is enforced at each prediction step to prevent the controller from generating non-passive behaviors that can cause human harm. To ensure the feasibility of the optimization problem under varying human forces, the non-negative slack variable $s(k)$ is presented. This allows temporary violations of the strict passivity condition which is penalized by a weighted term β introduced in the objective function to avoid overly stiff and energetically aggressive behavior which can negatively affect the user's comfort. The analysis used to evaluate the system's passivity during execution is presented as:

5) Passivity Analysis: To investigate the safety of the MPVA with varying stiffness and damping terms, the following storage function is considered as:

$$V = \frac{1}{2}\tilde{\boldsymbol{v}}^{p\top}_{r,d}\boldsymbol{K}^p_m\tilde{\boldsymbol{v}}^p_{r,d} + \frac{1}{2}\tilde{\boldsymbol{x}}^{p\top}_{r,d}\boldsymbol{K}^p_k\tilde{\boldsymbol{x}}^p_{r,d} \tag{12}$$

where $\frac{1}{2}\tilde{\boldsymbol{v}}^{p\top}_{r,d}\boldsymbol{K}^p_m\tilde{\boldsymbol{v}}^p_{r,d}$ represents the total scalar kinetic energy of the system, while $\frac{1}{2}\tilde{\boldsymbol{x}}^{p\top}_{r,d}\boldsymbol{K}^p_k\tilde{\boldsymbol{x}}^p_{r,d}$ represents the total scalar potential energy of the system. As $\boldsymbol{K}^p_m$ is constant and $\boldsymbol{K}^p_k$ is varying symmetric matrices, differentiating V and substituting with the admittance dynamics Eq. (2) leads to:

$$\dot{V} = \tilde{\boldsymbol{v}}^{p\top}_{r,d}\boldsymbol{f} + \left[\frac{1}{2}\tilde{\boldsymbol{x}}^{p\top}_{r,d}\dot{\boldsymbol{K}}^p_k\tilde{\boldsymbol{x}}^p_{r,d} - \tilde{\boldsymbol{v}}^{p\top}_{r,d}\boldsymbol{K}^p_d\tilde{\boldsymbol{v}}^p_{r,d}\right] \tag{13}$$

where $\dot{\boldsymbol{K}}^p_k$ is the rate of change of the varying stiffness parameter. The input power injected by the human user is defined as $\tilde{\boldsymbol{v}}^{p\top}_{r,d}\boldsymbol{f}$, the storage power is defined as $\frac{1}{2}\tilde{\boldsymbol{x}}^{p\top}_{r,d}\dot{\boldsymbol{K}}^p_k\tilde{\boldsymbol{x}}^p_{r,d}$, and the dissipated power is specified as $\tilde{\boldsymbol{v}}^{p\top}_{r,d}\boldsymbol{K}^p_d\tilde{\boldsymbol{v}}^p_{r,d}$. To guarantee that the total power of the system does not exceed the input power of the human, $\dot{V} \leq \tilde{\boldsymbol{v}}^{p\top}_{r,d}\boldsymbol{f}$, which leads to the passivity conditions $\frac{1}{2}\tilde{\boldsymbol{x}}^{p\top}_{r,d}\dot{\boldsymbol{K}}^p_k\tilde{\boldsymbol{x}}^p_{r,d} \leq \tilde{\boldsymbol{v}}^{p\top}_{r,d}\boldsymbol{K}^p_d\tilde{\boldsymbol{v}}^p_{r,d}$ [14]. This inequality is taken into account in the MPVA-TFP formulation, and the storage function can be used as a Lyapunov-like function to show the system's stability.

4. Experimental Results

To validate the effectiveness of the proposed architecture, a series of comparative experimental tests are conducted. The proposed optimization-based approach is compared to a heuristic-based approach that depends of Fuzzy Logic principle previously introduced through [10].

In this section, the heuristic-based adaptation method is presented briefly. Moreover, the experimental setup and tests are introduced. The obtained results are examined, highlighting the system's behavior under various conditions and diverse interactions.

A. Heuristic-based adaptation method

The heuristic adaptation strategy employed in this work is based on Fuzzy Logic principle which is an intelligent approach that mainly applies knowledge to manipulate the environment and learning from experience without depending on the system model [10]. This approach is used to update the stiffness $\boldsymbol{K}_k^p$ and accordingly the damping $\boldsymbol{K}_d^p$ parameters to guarantee a critically damped system. The inertia matrix $\boldsymbol{K}_m^p$ is kept constant as the robot moves with low velocities during the physical interaction, in addition to prevent possible sluggish or unstable behavior [16]. The fuzzy-based method used in this study considers each Cartesian coordinate separately, as the aforementioned gains are adapted in $[x, y, z]$ coordinates according to the Cartesian position tracking error $\tilde{\boldsymbol{x}}_{r,d} = [e_{x_{r,d}}, e_{y_{r,d}}, e_{z_{r,d}}]^T$, the magnitude of the applied external forces $|\boldsymbol{f}| = [|f_x|, |f_y|, |f_z|]^T$ and its direction towards the desired motion $\cos(\theta)$.

The membership functions used for both the inputs and the outputs are constructed as simple triangular sets defined as "Low", "Medium" and "High" inspired by those introduced in [10]. The fuzzy-based adaptation block can be integrated to the proposed architecture instead of the MPC-based Adaptation presented in Fig. 1.

Once the membership functions are defined, conditional fuzzy rules are constructed to map the interaction variables into appropriate admittance gains based on the problem's definition and experimentation. For instance, when the position error is classified as "High", the stiffness parameter of the corresponding axis is increased to compensate for the deviation and enforce path tracking. Similarly, the applied force and its directionality are interpreted, if the force magnitude is "High" and oriented in the opposite direction to the robot's motion; classified as "Low", consequently, the corresponding stiffness is set to "High" to resist the applied forces and follow the assigned track.

Nevertheless, if the forces magnitude is "High" aligned with the direction of motion classified as "High", then the stiffness is reduced to "Low" or "Medium", to allow the human-applied forces to contribute constructively to trajectory execution. Additional rules are formulated in a similar manner to cover all possible combinations of input conditions, ensuring a consistent and interpretable adaptation of the admittance parameters. The Mamdani method is selected to implement the adaptation model and the logical AND and OR operators are replaced with min(·) and max(·) respectively. The selected area centroid is obtained in the defuzzification process [10].

While the fuzzy-based adaptation provides an interpretable rule-driven mechanism for adjusting the admittance parameters, it may lead to abrupt changes and limited scalability in sudden and complex interaction dynamics.

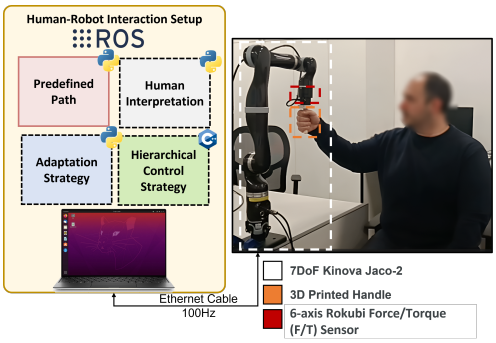

Fig. 2: The experimental platform

To address these limitations, the MPC-based variable admittance approach is proposed. Thus, these methods are analyzed and compared experimentally.

B. Experimental Setup

The experiments are performed utilizing a 7 DoF Kinova JACO-2 robot [17] equipped with 6-axis Rokubi force/torque (F/T) sensor with a sampling frequency of 100Hz [18] attached to its end-effector, joint encoders and torque sensors. The robot's gripper is replaced by a designed handle fabricated using 3D printing facilities, for easier human grasp in the pHRI application. Robot Operating System (ROS) is used to integrate the system components through ROS topics. The experimental platform is shown in Fig. 2. The reference trajectories are computed offline in advance and then utilized during the experiments as a periodic trajectory, which is dynamically generated based on the current position of the robot's end-effector grasped by the human subject. This facilitates a smooth trajectory following behavior that adapts in real-time based on the pHRI. Two representative interaction paths are employed to evaluate the framework. The first is a periodic straight-line path, used to compare controllers across human subjects through three control methods:

- **Method 1:** Fixed gain admittance control divided into two configurations: low-gain (FLA) and high-gain (FHA). These configurations are used as baseline for the comparison [19].
- **Method 2:** Fuzzy-based variable admittance (FVA), employing rule-based inference system using tracking error and interaction forces to adapt stiffness gains in real-time [10].
- **Method 3:** Model predictive variable admittance with tracking error and interaction forces accounting for passivity conditions (MPVA). With the integrated force direction and passivity constraints, the admittance parameters are adjusted considering compliance while maintaining safety.

Human subjects are instructed to move along the path for the 1^{st} two cycles, providing the robot with assistive forces. During the last 3^{rd} cycle, the subjects are requested to induce resistive forces opposing the robot's direction of motion to validate the architecture in different physical interaction modes. The second path is a rehabilitation-inspired 3D path, designed to mimic complex upper limb motions utilized to validate the heuristic fuzzy-based and optimal MPVA strategies. These paths enable broad benchmarking of all methods and focused evaluation of the most advanced controllers in realistic rehabilitation scenarios.

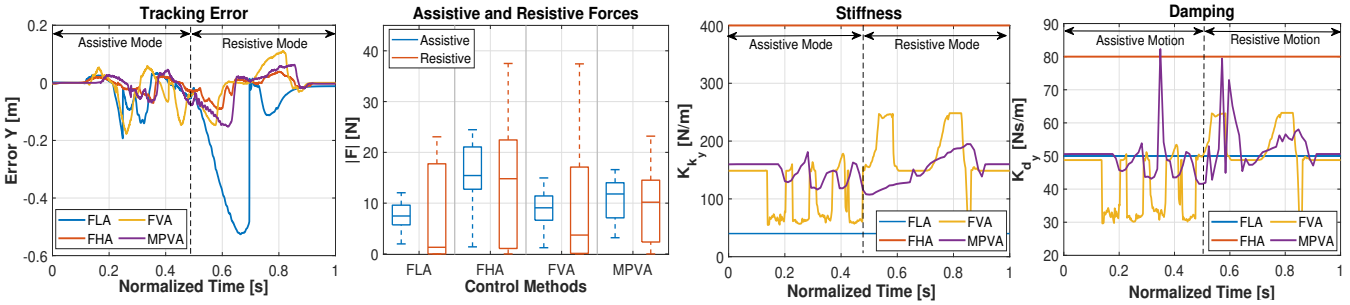

(a) Tracking error (b) Force distribution (c) Stiffness (d) Damping

Fig. 3: Motion deviation, force distribution, stiffness and damping parameters of one subject in assistive and resistive modes

TABLE I: Straight line path evaluation metrics for all control methods

Controller/Metric	$RMSE$ $[m]$	MAE $[m]$	$\|F\|$ $[N]$	$\|\dot{K}_k^p\|$ $[N/m]$	P_{in} $[W]$		P_{out} $[W]$		T_{comp} $[s]$
					MEAN	MAX	MEAN	MAX	
FLA	0.174	0.101	6.26	N/A	0.65	4.88	-0.45	0.0	0.01
FHA	0.03	0.021	10.53	N/A	0.65	7.23	-0.33	0.0	0.01
FVA	0.062	0.042	7.34	42.6	0.67	5.99	-0.34	1.94	0.1
MPVA	0.053	0.037	7.16	9.48	0.65	4.96	-0.34	0.03	0.5

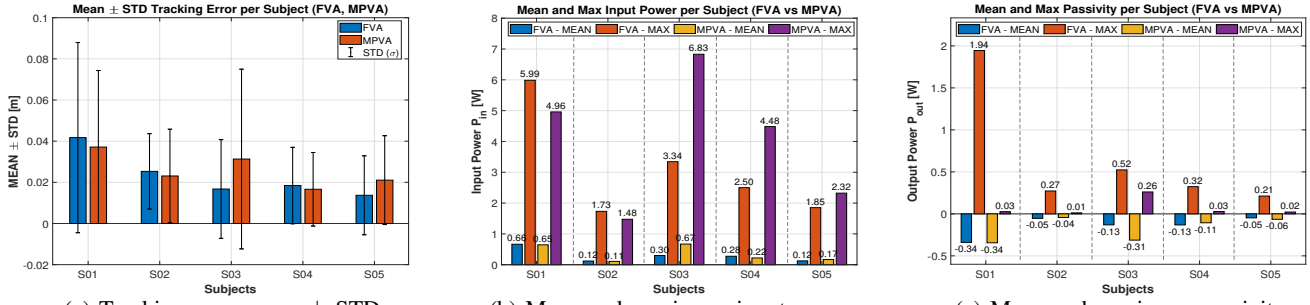

(a) Tracking error mean ± STD (b) Mean and maximum input power (c) Mean and maximum passivity

Fig. 4: Mean error and STD, average and maximum input power and passivity over all subjects across controllers

The controllers performance is evaluated using both quantitative metrics (e.g., root mean square tracking error, mean interaction forces) and subjective feedback obtained through post-experiment surveys. The control setting parameters are selected experimentally, FLA gains are set to $K_k = 40$ and $K_d = 50$, and FHA gains are $K_k = 400$ and $K_d = 80$. These values are determined experimentally to achieve a critically damped to overdamped response, ensuring fast and stable performance away from the resonance phenomenon that can affect the hardware. For MPVA, $Q = Q_n = 0.1$, $R_{K_k} = R_{K_d} = 0.01$, $\beta = 5$, $N_p = 20$, and the stiffness bounds are set to $K_{min} = 20$ and $K_{max} = 300$. The mass matrix $K_m = 4$ is kept constant for all controllers. The gains and weighting matrices are diagonal matrices with identical diagonal elements as specified.

C. Results on the Straight-Line Path

The periodic straight-line path is first evaluated by one representative subject moving in the Y-direction to analyze system's performance in a repeatable interaction setting under all control methods in both assivitive and resistive modes. As shown in Figs. 3a and 3b and demonstrated through the summarized evaluation metrics in Table I, FLA showed the highest tracking error with a root mean square error (RMSE) of 0.174m and mean absolute error of 0.1m due to low gains, which offer minimal opposition to human-applied forces with an average of 6.26N and a maximum of 12.05N and 23.06N in assistance and resistance, respectively. FHA improved accuracy substantially with RMSE of 0.03m and MAE of 0.021m, however, it exhibits the highest force distribution as shown in Fig. 3b with a mean of 10.53N, reflecting higher physical effort. The fuzzy-based variable admittance (FVA) reduced the tracking error compared to FLA of a RMSE of 0.062m and MAE of 0.042m and maintained moderate forces of an average of 7.34N.

However, its rule-based adaptation led to abrupt changes in stiffness and correspondingly damping gains as shown in Figs. 3c and 3d of $|\dot{K}_k^p| = 42.6$Ns/m, which in turn produced higher force peaks as shown in Fig. 3b. Its maximum output power is of 1.94W corresponding to 32% of the maximum input power, indicating a significant energy injection.

In contrast, the proposed MPVA achieved comparable accuracy with RMSE of 0.053m and MAE of 0.037m with relatively lower force distribution in both assistive and resistive modes with a mean of 7.16N, with smoother stiffness adaptation as shown through Fig. 3c of $|\dot{K}_k^p| = 9.48$Ns/m. Importantly, MPVA maintained passivity with a negligible maximum output power of 0.03 W, representing 0.6% of the maximum input power.

As shown in Figs. 3c and 3d, the MPVA adaptation occasionally increased damping sharply to compensate for stiffness variations and ensure passivity. These abrupt damping corrections are not perceptible to the human subject due to task low motion speed.

Although the computational load of MPVA is approximately five times higher than that of FVA, with a frequency of 2Hz compared to 100Hz frequency of the overall control loop. However, this frequency is within the bandwidth of comfortable and sustainable interaction, as higher rates become challenging for human coordination. For a deeper comparison between the adaptive schemes, the experiment is conducted by five male subjects aged from 29 to 42 years, with average weight of 78kg and height 1.75m under both FVA and MPVA. The collective results are presented in Fig.4, which shows the mean and standard deviation (STD) of the tracking error, the average input power ($\tilde{\boldsymbol{v}}_{r,d}^{p\top}\boldsymbol{f}$), and the output power ($\frac{1}{2}\tilde{\boldsymbol{x}}_{r,d}^{p\top}\dot{\boldsymbol{K}}_k^p\tilde{\boldsymbol{x}}_{r,d}^p - \tilde{\boldsymbol{v}}_{r,d}^{p\top}\boldsymbol{K}_d^p\tilde{\boldsymbol{v}}_{r,d}^p$), which reflects the system's passivity across all subjects.

Figs. 4a–4c and Table II present the results of five subjects performing the straight-line path under FVA and MPVA. Both controllers achieved nominal trajectory performance, with mean RMSE below 0.04m; however, MPVA showed slightly higher errors than FVA in some subjects, reflecting the trade-off introduced by its optimization and safety constraints. This difference in accuracy is accompanied by distinct interaction dynamics. MPVA required marginally higher average input forces 5.66N vs. 5.0N for FVA and occasionally higher input power in individual subjects (e.g., S03 and S04). Despite these variations, the most significant distinction lies in passivity behavior, where FVA produced clear violations, with output power excursions up to 1.94W, whereas MPVA consistently kept output power near zero with smaller deviations (e.g., 0.26W for S03). These results highlight that while MPVA may yield slightly higher tracking error in some cases, it provides smoother adaptation and robust passivity guarantees, ensuring safer and more stable interaction compared to FVA.

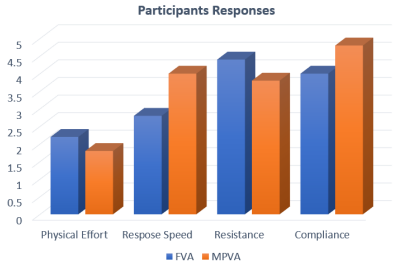

Fig. 5: NASA task load index (NASA TLX) responses

TABLE II: Average evaluation metrics per controller

Controller/Metric	$RMSE$ [m]	MAE [m]	$\lvert F\rvert$ [N]	$\lvert \dot{K}_k^p\rvert$ [N/m]
FVA	0.035	0.023	5.0	43.48
MPVA	0.039	0.026	5.66	10.04

To assess subjects' feedback on effort, comfort, and assistance, a post-experiment survey based on the NASA task load index (NASA TLX) is used to measure and conduct a subjective mental workload (MWL) assessment [20]. Subjects feedback shown in Fig. 5 reflects that MPVA achieves high compliance ratings, while avoiding excessive resistance as in FVA, as it prioritizes human safety and avoids sudden resistive responses. It maintains relatively low physical effort and a higher response speed than the FVA.

Four out of five subjects recommended the MPVA over the FVA as the most suitable control method for pHRI. A supplementary demonstration video can be accessed through: https://youtu.be/IBlON_KxrXY. Further analysis and experiments are presented through our previous paper [21].

D. Results on the Rehabilitation-Inspired 3D Path

The rehabilitation-inspired three-dimensional (3D) path is based on the Proprioceptive Neuromuscular Facilitation (PNF) pattern, which is one of the methods used for upper and lower limbs rehabilitation [22]. Focusing on the upper extremity pattern, the PNF pattern is represented by a sequence of flexion-extension, abduction-adduction, and internal-external rotation of the joints, which is selected to be analyzed in this study for shoulder rehabilitation starting by shoulder flexion, adduction and external rotation, forearm supination, wrist flexion and finger flexion, and ending by shoulder extension, abduction and external rotation, forearm pronation, wrist and finger extension. To construct the PNF pattern, the position of human's wrist joint in 3D space is estimated with respect to the human's fixed hip joint. This estimation is constructed using a stereovision setup for depth estimation process. The human pose is estimated utilizing MediaPipe Pose (MPP) which is an open-source cross-platform framework that relies on lightweight Machine Learning (ML) architecture that extracts 33 2D human body landmarks for real-time human joint pose estimation [10]. The arm's wrist and hip landmarks are used to estimate the wrist's position with respect to the hip joint.

The estimated position is then transformed from the camera frame to the manipulator's fixed base global frame for tracking purposes.The estimated trajectory is then filtered using Savitzky-Golay smoothing filter which depends on fitting successive sub-sets of adjacent data points defined as a window with a polynomial of degree n using linear least squares method. The process of wrist trajectory estimation is shown through Fig. 6.

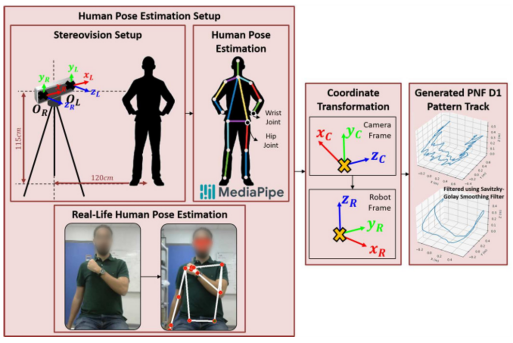

Fig. 6: Wrist pose estimation for PNF path generation

The 3D rehabilitation-inspired PNF path is tested for further analysis by a single subject to evaluate the controllers behavior in complex motion. Both FVA and MPVA closely follow the reference as shown in Fig. 7a, with RMSE of 0.046m and 0.048m, respectively. Passivity analysis in Fig. 7c shows that FVA exhibited clear violations, reaching up to 0.53W at the highlighted points, while MPVA remained near zero with a maximum of 0.01W.

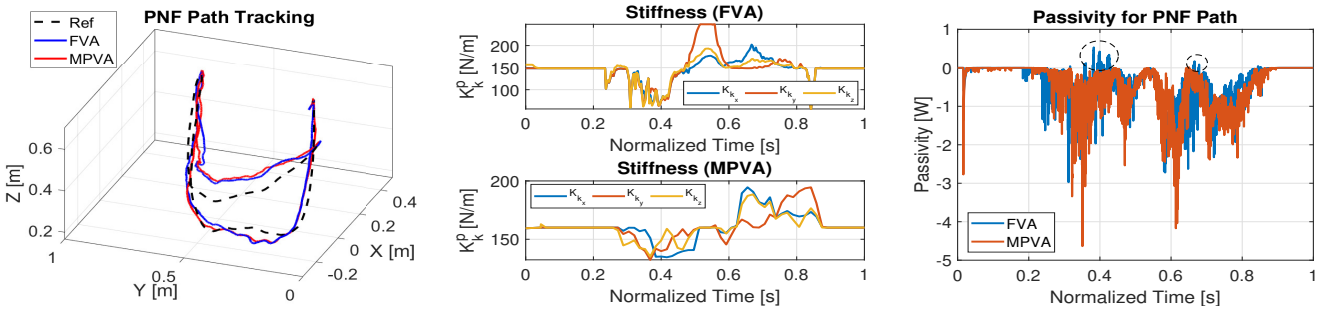

(a) Tracking error (b) Stiffness (c) Passivity

Fig. 7: PNF tracking error, stiffness evolution and output power (passivity) across controllers

The stiffness evolution shown in Fig. 7b further confirms this trend as FVA shows abrupt changes of a mean $|\dot{K}_k^p|$ of 46.8Ns/m, whereas MPVA maintains smoother adaptation of 6.43Ns/m. These results confirm that, while both achieve accurate tracking, MPVA ensures safer and more stable interaction by regulating energy exchange.

5. Conclusions

This work proposed a novel real-time Model Predictive Variable Admittance (MPVA) control architecture for safe and high-performance pHRI. The framework adaptively tunes the admittance parameters via MPC, optimizing tracking error, interaction force magnitude, and direction for intent-aware behavior, while embedding passivity constraints to ensure safety and prevent sudden resistive responses. The scheme is validated experimentally against other algorithmic baselines, including a fixed-gain admittance and a fuzzy-based adaptive admittance control approaches on a group of 5 subjects. The results demonstrate the effectiveness of the proposed method, showing context-aware gain adaptation, safe interaction, and reduced energy injection, supported by objective metrics and NASA TLX evaluations.

For future endeavors, it is recommended to enhance the system's ability to capture the human intention, including other sensor types such as RGB-D cameras or ElectroMyoGraphyc (EMG) sensors, as well as employing data-driven approach to enhance generability of the approach.

References

[1] J. Luo, C. Zhang, W. Si, Y. Jiang, C. Yang, and C. Zeng, "A physical human–robot interaction framework for trajectory adaptation based on human motion prediction and adaptive impedance control," *IEEE Transactions on Automation Science and Engineering*, vol. 22, pp. 5072–5083, 2024.

[2] C. Véronneau, J. Denis, L.-P. Lebel, M. Denninger, V. Blanchard, A. Girard, and J.-S. Plante, "Multifunctional remotely actuated 3-dof supernumerary robotic arm based on magnetorheological clutches and hydrostatic transmission lines," *IEEE Robotics and Automation Letters*, vol. 5, no. 2, pp. 2546–2553, 2020.

[3] M. Bednarczyk, H. Omran, and B. Bayle, "Model predictive impedance control," in *2020 IEEE International Conference on Robotics and Automation (ICRA)*, 2020, pp. 4702–4708.

[4] A. Madani, P. P. Niaz, and e. a. Guler, "Robot-assisted drilling on curved surfaces with haptic guidance under adaptive admittance control," in *2022 IEEE/RSJ International Conference on Intelligent Robots and Systems (IROS)*. IEEE, 2022, pp. 3723–3730.

[5] L. Han, L. Zhao, Y. Huang, and W. Xu, "Variable admittance control for safe physical human–robot interaction considering intuitive human intention," *Mechatronics*, vol. 97, p. 103098, 2024.

[6] D. M. Mahfouz, O. M. Shehata, E. I. Morgan, and F. Arrichiello, "A comprehensive review of control challenges and methods in end-effector upper-limb rehabilitation robots," *Robotics*, vol. 13, no. 12, p. 181, 2024.

[7] J. Chen and P. I. Ro, "A conceptual approach of passive human-intention-orientated variable admittance control using power envelope," in *2021 IEEE/RSJ International Conference on Intelligent Robots and Systems (IROS)*. IEEE, 2021, pp. 7300–7306.

[8] W. Zou, P. Duan, Y. Chen, N. Yu, and L. Shi, "Variable stiffness control with strict frequency domain constraints for physical human-robot interaction," in *2020 IEEE/RSJ International Conference on Intelligent Robots and Systems (IROS)*. IEEE, 2020, pp. 7146–7151.

[9] Z. Li, H. Huang, X. Song, W. Xu, and B. Li, "A fuzzy adaptive admittance controller for force tracking in an uncertain contact environment," *IET control theory & applications*, vol. 15, no. 17, pp. 2158–2170, 2021.

[10] D. M. Mahfouz, P. Di Lillo, O. M. Shehata, E. I. Morgan, and F. Arrichiello, "Development of a fuzzy-based adaptive admittance control architecture for upper limb robotic rehabilitation," in *2024 IEEE International Conference on Robotics and Biomimetics (ROBIO)*. IEEE, 2024, pp. 148–153.

[11] N. Thelenberg and C. Ott, "On handling variable stiffness parameters in compliance control via mpc," in *2024 European Control Conference (ECC)*. IEEE, 2024, pp. 615–620.

[12] A. S. Anand, J. T. Gravdahl, and F. J. Abu-Dakka, "Model-based variable impedance learning control for robotic manipulation," *Robotics and Autonomous Systems*, vol. 170, p. 104531, 2023.

[13] K. Haninger, C. Hegeler, and L. Peternel, "Model predictive impedance control with gaussian processes for human and environment interaction," *Robotics and Autonomous Systems*, vol. 165, 2023.

[14] M. Bednarczyk, H. Omran, and B. Bayle, "Passivity filter for variable impedance control," in *2020 IEEE/RSJ International Conference on Intelligent Robots and Systems (IROS)*. IEEE, 2020, pp. 7159–7164.

[15] P. Di Lillo, D. Di Vito, and G. Antonelli, "Merging global and local planners: real-time replanning algorithm of redundant robots within a task-priority framework," *IEEE Transactions on Automation Science and Engineering*, vol. 20, no. 2, pp. 1180–1193, 2022.

[16] L. Zhang, S. Guo, and Q. Sun, "An assist-as-needed controller for passive, assistant, active, and resistive robot-aided rehabilitation training of the upper extremity," *Applied Sciences*, vol. 11, no. 1, p. 340, 2020.

[17] K. , "Discover our Gen2 robots | Kinova," https://www.kinovarobotics.com/product/gen2-robots, may 10 2023.

[18] "Rokubi 6-axis Force Torque Sensor | Bota Systems," https://www.botasys.com/force-torque-sensors/rokubi, [Accessed 03-2024].

[19] R. S. Zarrin, A. Zeiaee, and R. Langari, "A variable-admittance assist-as-needed controller for upper-limb rehabilitation exoskeletons," *IEEE Robotics and Automation Letters*, vol. 9, no. 6, pp. 5903–5910, 2024.

[20] S. G. Hart, "Nasa-task load index (nasa-tlx); 20 years later," in *Proceedings of the human factors and ergonomics society annual meeting*, vol. 50, no. 9. Sage publications Sage CA: Los Angeles, CA, 2006, pp. 904–908.

[21] D. M. Mahfouz, P. D. Lillo, O. M. Shehata, E. I. Morgan, and F. Arrichiello, "Passivity-constrained model predictive variable admittance control for safe and adaptive physical human–robot interaction," *IEEE Robotics and Automation Letters*, pp. 1–8, 2026.

[22] P. Chaturvedi, A. K. Singh, D. Kulshreshtha, and A. K. Thacker, "Pnf in acute stroke," *MOJ Anat & Physiol*, vol. 5, pp. 391–399, 2018.